Contents lists available at ScienceDirect

Transactions of Nonferrous Metals Society of China

36(2026) 740−753

www.tnmsc.cn

Interpretable machine learning predictive model for mechanical properties of AZ31 magnesium alloy rolled sheets

Bi-wu ZHU [a,b], Hao JIANG [b], Qiu-ping YI [c,*], Xiao LIU [a,b,d,**], Jian-zhao WU [a], Wen-hui LIU [a,b], Cong-chang XU [d], Luo-xing LI [d], Ke HU [e]

[a] College of Marine Equipment and Mechanical Engineering, Jimei University, Xiamen 361021, China;
[b] Hunan Engineering Research Center of Forming Technology and Damage Resistance Evaluation for High-Efficiency Light Alloy Components, Hunan University of Science and Technology, Xiangtan 411201, China;
[c] College of Finance and Economics, Jimei University, Xiamen 361021, China;
[d] Research Institute of HNU in Chongqing, Hunan University, Chongqing 401135, China;
[e] School of Materials Science and Engineering, Guangdong Ocean University, Yangjiang 529500, China

Abstract: To investigate the complex relationship between rolling process parameters and mechanical properties of AZ31 magnesium alloy rolled sheets, the Leave-One-Out Cross-Validation (LOOCV) and parameter tuning were applied to optimizing hyper-parameters for the four (BPNN, SVR, RF, and KNN) machine learning models. An interpretable prediction model based on machine learning and SHapley Additive exPlanations (SHAP), as well as an analytical method combining the SHAP model and the Pearson Correlation Coefficient (PCC), were proposed. The results showed that among the four models, the SVR model was able to simultaneously and accurately predict the ultimate tensile strength (UTS) and elongation (EL). According to the combination analysis of PCC and the magnesium alloy rolling forming mechanism, it was found that strain rate and reduction displayed a negative and positive correlation with UTS, respectively, while rolling temperature and reduction illustrated a positive and negative correlation with EL, respectively. Through the SHAP method, which could interpret the output results of the SVR machine learning model, it was deduced that reduction and strain rate played an important role in the SVR model of the outputs of the UTS and EL, respectively. Combining SHAP with PCC, it was found that strain rate and reduction had a greater influence on the UTS than rolling temperature, whereas strain rate and rolling temperature had more influence on the EL compared to reduction.

Keywords: AZ31 magnesium alloy; rolling process; mechanical properties; machine learning; SHapley Additive exPlanations

1 Introduction

Magnesium alloys with outstanding physical properties, including low density, high specific strength, and stiffness, are recognized as environmentally friendly engineering materials and extensively utilized in various fields such as transportation, aerospace, communications, and electronics in the 21st century [1−4]. However, magnesium alloys have bottlenecks such as poor strength−plasticity matching and low forming efficiency, which limit their practical applications [5−8]. In recent years, researchers [9−12] have developed a single-pass medium-to-high-strain-rate roll forming technology, which boasts high forming efficiency. However, due to the intricate mapping relationships between process parameters and mechanical properties, existing physical models are less capable of accurately predicting these properties. Hence, there

Corresponding author: *Qiu-ping YI, Tel: +86-13739078968, E-mail: easy@jmu.edu.cn;
**Xiao LIU, Tel: +86-18674355539, E-mail: liuxiao0105@163.com
https://doi.org/10.1016/S1003-6326(25)66994-9
Received 13 June 2024; accepted 20 March 2025

is an urgent need to explore a new approach to establish the relationship between the single-pass medium-to-high-strain-rate rolling process and mechanical properties to achieve accurate prediction of mechanical properties.

In recent years, machine learning has been frequently employed to predict the mechanical properties of metallic materials. Machine learning has no fixed rules, and the training of its algorithms and models allows it to automatically learn and extract regularities in the data to make optimal decisions and predictions [13−16]. FAN et al [17] utilized ResNet (Residual Neural Network), GBDT (Gradient Boosting Decision Tree), and LGB (Light Gradient Boosting) machine learning models with good generalization ability and prediction accuracy to forecast the fatigue strength of six materials, including steel, Ni-based SC alloys, and Ni-based DS alloys, which were widely applied in aerospace applications. The predicted results were consistently within the ±10% error band across various material types, stress ratios, and crystal orientations. LI et al [18] predicted the hardness, yield strength (YS), and ultimate tensile strength (UTS) of multi-principal element alloys (MPEAs) employing RF (random forest), KNN (K-nearest neighbor), SVR (support vector regression), and ANN (artificial neural network) machine learning models. However, the models exhibited poor performance in the prediction of the elongation (EL) for the MPEAs, with the coefficient of determination (R^2) ranging from 0.295 to 0.487. SUH et al [19] employed an optimized ANN to predict the tensile yield strength (TYS), compressive yield strength (CYS), and yield asymmetry (YA) of extruded Mg−Al−Zn−Mn−Ca−Y alloys based on R^2. The predicted models demonstrated good performance on the training, validation, and test sets. XU et al [20] utilized ANN and SVR learning models to predict the mechanical properties of AZ31 magnesium alloy and found that the predicted models for the YS and UTS showed fine accuracy, but the EL could not be exactly predicted. DONG et al [21] applied machine learning models to predict the mechanical properties based on experimental data from published literature and pointed out that the optimal prediction models for UTS, YS, and hardness exhibited high accuracy, with R^2 exceeding 0.8 and reaching a maximum value of 0.93. However, the prediction model for EL performed poorly, with an R^2 of 0.71. In general, there have been many researchers who have studied the application of machine learning in predicting mechanical properties in the field of materials. Their models perform better in predicting most of the mechanical properties, but the correlation coefficients are low, and the prediction accuracy is low in EL prediction.

Traditional trial-and-error methods require a large amount of computational resources and time, which are prone to overfitting. In contrast, finding hyper-parameters by Leave-One-Out Cross-Validation (LOOCV) can address these issues, and it can efficiently select better parameter combinations without needing to try a large number of combinations to avoid overfitting the training set [22−24]. In addition, the Pearson Correlation Coefficient (PCC) is commonly used to analyze the relationship between variables. However, PCC can only capture linear relationships [25]. While the SHapley Additive exPlanations (SHAP) can help us to better understand the non-linear relationships among variables [26−28]. By calculating SHAP values, the degree of influence of the variables on the model predictions can be obtained, which in combination with PCC allows for a more comprehensive assessment of the relationship between process parameters and the mechanical properties.

In this study, we established relationship models between medium-to-high-strain-rate rolling parameters in a single pass and mechanical properties in AZ31 magnesium alloy sheets using four commonly used machine learning methods (BPNN, SVR, RF, and KNN), and determined the optimized parameters of the four machine learning models by the LOOCV and parameter tuning. The machine learning model that could simultaneously and accurately predict UTS and EL was obtained. The correlation between the rolling process and the mechanical properties was illustrated using the PCC in conjunction with magnesium alloy rolling and forming theory. The analytical findings of the PCC were validated and complemented by the SHAP method, while the SVR model with superior predictive capabilities was elucidated. The research presented in this study offers new insights for optimizing the single-pass medium-to-high-strain-rate rolling process and adjusting the mechanical properties of commercial AZ31 magnesium alloy.

2 Methods

2.1 Source and processing of data

2.1.1 Data acquisition and sample noise removal

The original data for the medium-to-high-strain-rate rolling of AZ31 magnesium alloy used in this study were sourced from our previous research [29−31]. The presence of noise and outliers in a general sample leads to significant variability in distribution. Therefore, data preprocessing is essential to ensure the accuracy of prediction results [32,33]. In this study, the Pauta criterion is employed to eliminate outliers and discrete points, based on the theory of data normal distribution [34]. The upper limit of the confidence interval is set as $\overline{y}+3S_y$, and the lower limit of the confidence interval is set as $\overline{y}-3S_y$. Data points exceeding three times the standard deviation are identified as outliers and subsequently removed. The Pauta criterion is defined by Eqs. (1)−(3) [34]:

$$\left|y_i-\overline{y}\right|>3S_y \tag{1}$$

$$\overline{y}=\frac{1}{N}\sum_{i=1}^{N}y_i \tag{2}$$

$$S_y=\sqrt{\frac{1}{N}\sum_{i=1}^{N}\left(y_i-\overline{y}\right)^2} \tag{3}$$

where y_i is the sample value with i=1, 2, 3, ···, N, $\overline{y}$ is the mean value of y, S_y is the standard deviation value of the sample, and N is the total number of samples.

Following this guideline, a total of 32 sets of rolling data were ultimately chosen as the dataset for the machine learning model. Subsequently, approximately 80% of the data, equivalent to 25 sets, were randomly selected as the training samples to ensure the prediction accuracy of the model. Additionally, about 20% of the data, including 7 sets, were designated as the prediction samples to validate the predictive performance of the model. All data are presented in Table 1.

2.1.2 Data standardization

Due to the disparity in magnitudes among the input feature variables, directly feeding them into the model for training may result in slow convergence or even failure to converge. To address the impact of varying feature magnitudes and facilitate the training of the machine learning model, data normalization is necessary [35−37]. The sample data are normalized using the following equation [36]:

$$x=\frac{x_0-x_{\min}}{x_{\max}-x_{\min}} \tag{4}$$

where x is the normalized data, x_0 is the original data, $x_{\min}$ is the minimum value in the original data, and $x_{\max}$ is the maximum value in the original data.

Table 1 Data for rolled plate samples

Sample No.	Rolling temperature/°C	Strain rate/s^{-1}	Reduction/%	UTS/MPa	EL/%
1	300	10.0	80	245.0	13.1
2	300	15.0	80	249.0	14.0
3	300	20.0	80	254.0	17.7
4	350	10.0	80	252.0	15.0
5	350	15.0	80	245.0	14.3
6	350	20.0	80	246.0	14.9
7	370	1.5	50	234.8	11.4
8	370	1.9	75	294.3	13.5
9	370	4.8	75	275.9	15.5
10	370	6.5	50	232.7	17.3
11	370	7.8	75	267.0	18.8
12	400	10.0	80	253.0	12.4
13	400	15.0	80	252.0	15.3
14	400	20.0	80	250.0	18.3
15	410	1.9	75	294.0	18.3
16	410	4.0	50	251.4	19.5
17	410	4.8	75	280.0	21.7
18	410	6.5	50	252.7	22.8
19	410	7.8	75	264.0	24.1
20	430	1.9	50	217.3	18.69
21	430	3.0	50	209.4	18.28
22	430	4.0	50	237.2	19.19
23	430	4.8	50	241.2	21.25
24	430	5.6	50	247.3	21.83
25	430	1.9	75	287.0	15.14
26	430	3.0	75	278.1	19.94
27	460	1.5	50	251.5	13.0
28	460	1.9	75	275.0	13.2
29	460	4.0	50	232.5	16.8
30	460	4.8	75	261.0	16.6
31	460	6.5	50	239.8	24.2
32	460	7.8	75	259.6	21.0

2.2 Four machine learning models

2.2.1 BPNN

The BPNN is a multilayer feed-forward neural network trained using the error back-propagation algorithm and is one of the most commonly utilized neural network models. It comprises multiple neurons typically organized into three layers: the input layer, hidden layer, and output layer [38−40]. The fundamental principle of the BPNN is the gradient descent method, employing gradient search techniques to minimize the mean square deviation between the actual output value and the desired output value of the network. The topological model of the BPNN is illustrated in Fig. 1.

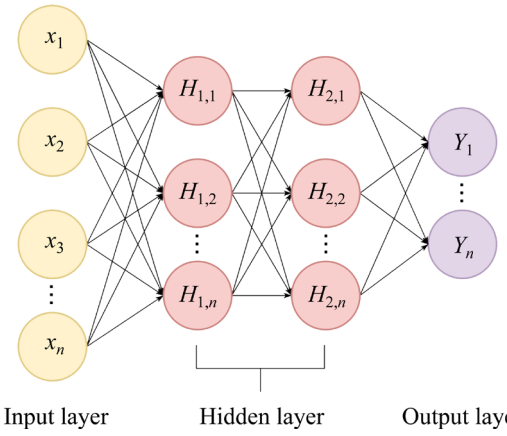

Fig. 1 Topology of BPNN

The parameters, including the input layer, output layer, hidden layer, and activation function, are required to establish the BPNN model. The BPNN model generally adopts the tansig activation function, which performs better when the feature differences are significant and enhances the effect of feature expansion during the iteration. The tansig activation function (tansig(x)) is represented by the following equation [41]:

$$\text{tansig}(x)=\frac{2}{1+\mathrm{e}^{-2x}}-1 \tag{5}$$

2.2.2 SVR

The SVR is a supervised learning model, primarily employed for classification and regression analysis. It is adept at categorizing data into distinct classes or forecasting continuous target values based on their attributes [42,43]. The fundamental concept involves mapping input vectors to a high-dimensional space where the data are segregated into two classes. By identifying a hyperplane to differentiate the two classes of data, SVR accomplishes data classification.

When the SVR model is utilized to address problems, it is essential to introduce a suitable kernel function based on the characteristics of the problem. The kernel function can reflect the distribution characteristics of the training samples. Given that predicting the mechanical properties of rolled plates involves a nonlinear problem, it is crucial to incorporate a nonlinear kernel function. In this study, the RBF function is selected as the kernel function, and the nonlinear regression expression of the SVR is given in Eq. (6) [44]:

$$f(x)=\sum_{i=1}^{m}\left(\hat{a}_i-a_i\right)K\left(x,x_i\right)+b \tag{6}$$

where $\hat{a}_i$ is the Lagrange multiplier associated with the upper deviation, a_i is the Lagrange multiplier associated with the lower deviation, b is the model parameter, and $K(x, x_i)$ is the RBF kernel function with Eq. (7) [44]:

$$K\left(x,x_i\right)=\exp\left(-\frac{\left\|x-x_i\right\|^2}{2\delta^2}\right) \tag{7}$$

where δ is the bandwidth parameter.

The SVR model has two very important parameters, namely C and γ. C is the penalty coefficient, which represents the tolerance for error. A larger value of C indicates less tolerance for errors, which can lead to overfitting, while a smaller value can result in underfitting. Both excessively large and small values of C can lead to a decrease in the generalization ability of the SVR model. γ is a parameter that comes with the RBF function after the function is selected as the kernel function, which implicitly determines the distribution of the data after it is mapped to the new feature space. The larger the value of γ is, the fewer the support vectors there are, and the smaller the value of γ, the more the support vectors there are. The number of support vectors affects the speed of training and prediction.

2.2.3 RF

The RF is a classifier that applies multiple trees to train and predict samples. The “Random Forest” consists of two important keywords: “Random” and “Forest”. The “Random” refers to the random selection of samples and features, while the “Forest” indicates that the model comprises numerous decision trees. For an input sample, N trees will

produce N classification results, and RF aggregates all classification voting results, designating the class with the highest number of votes as the final output [45−47]. The flowchart of RF is shown in Fig. 2.

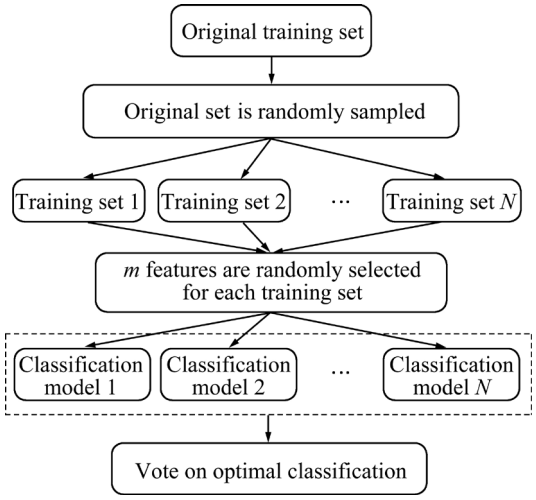

Fig. 2 RF algorithm flowchart

The accuracy of the RF model is influenced by the number of decision trees it comprises. The number of decision trees can be adjusted to improve the capacity of the model. The depth of the tree determines the complexity and classification precision of the model and can be adjusted to enhance the capability of the model.

2.2.4 KNN

The KNN is a versatile machine learning model with numerous applications. The distance between a new sample and each sample in the training set is calculated, and then the K nearest samples are selected as their neighbors. The category of the new sample is determined based on the categories of these neighbors. Here, K typically represents an integer not exceeding 20 [48−50]. The key parameters of the KNN model are the value of K and the distance metric. Its characteristics are simplicity, intuitiveness, ease of implementation, and in some cases, it exhibits excellent classification performance.

The Euclidean distance is the most common distance metric, measuring the absolute distance between two sample points in a multi-dimensional space [50]. Assuming the dimension of the multi-dimensional space is N, and $x_1=x_{11}, x_{12}, \cdots, x_{1N}$, and $x_2=x_{21}, x_{22}, \cdots, x_{2N}$ are two sample points, the Euclidean distance calculation formula between point x_1 and point x_2 is expressed by Eq. (8) [51]:

$$L_2(x_1,x_2)=\sqrt{\sum_{n=1}^{N}(x_{1n}-x_{2n})} \tag{8}$$

2.3 Building and evaluating machine learning models

2.3.1 Construction of machine learning models

In this study, four machine learning models were developed using MATLAB to predict the mechanical properties of AZ31 magnesium alloy plates rolled at medium-to-high-strain-rate. The establishment of the machine learning model is depicted in Fig. 3.

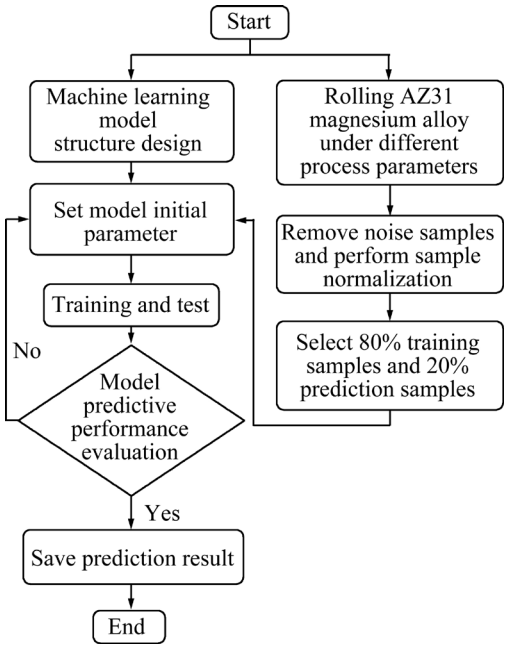

Fig. 3 Flowchart of establishing machine learning models

Since it is time-consuming and difficult to find the optimal hyper-parameters of the model when the traditional trial-and-error method is used to determine the hyper-parameters, and if the hyper-parameters are found to give the best predictive ability of the model, it is also possible to overfit the model. Therefore, the method of combining the LOOCV with hyper-parameter tuning is employed to solve the above problems so that the model has a satisfactory predictive ability. This approach can avoid overfitting and improve the generalization ability of the model. The determination of the optimal combination of the hyper-parameters is shown in Fig. 4.

The LOOCV is a common approach used for model evaluation, especially suitable for a small dataset. It evaluates the performance of the model by

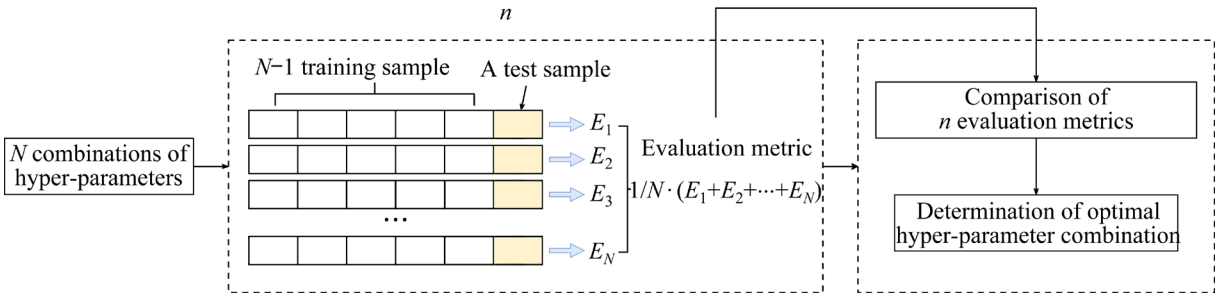

Fig. 4 Schematic diagram of LOOCV combined with hyper-parameter tuning

taking one sample from the dataset as the test sample and the remaining samples as the training samples, and this process continues until each sample has been used as a test sample once, resulting in n evaluation metrics (the evaluation metric chosen here is mean squared error (MSE)). The performance of the model is assessed based on the average of n evaluation metrics. In each LOOCV, the model is trained and evaluated for different combinations of hyper-parameters, and then the best-performing combination of hyper-parameters is selected based on the average evaluation metrics, where N is the total number of evaluations. By iterating this process repeatedly, the best hyper-parameter combination can eventually be found. In this study, the optimal hyper-parameters were determined by the LOOCV combined with hyper-parameter tuning, and the hyper-parameters for constructing the machine learning model are provided in Table 2.

Table 2 Hyper-parameters of machine learning models

Model	Parameter	Value
BPNN	Hidden layer sizes	(1, 8)
	Activation function	tansig
	Epoch	1000
	Learning rate	0.01
	Train minimum error	0.0001
SVR	Penalty factor, C	2
	Gamma, γ	1.7
RF	Number of trees	100
	Number of leaves	5
KNN	Number of neighbors	2

2.3.2 Evaluation of machine learning models

The prediction performance of machine learning models is primarily evaluated by calculating the mean absolute error (MAE), mean relative error (MRE), MSE, and R^2 between the predicted data and the experimental data of the models. The expressions are given in the following equations [52]:

$$\mathrm{MAE}=\frac{1}{N}\sum_{i=1}^{N}\left|\hat{y}_i-y_i\right| \tag{9}$$

$$\mathrm{MRE}=\frac{1}{N}\sum_{i=1}^{N}\left|\frac{\hat{y}_i-y_i}{y_i}\right|\times 100\% \tag{10}$$

$$\mathrm{MSE}=\frac{1}{N}\left(\hat{y}_i-y_i\right)^2 \tag{11}$$

$$R^2=1-\frac{\sum_{i=1}^{N}\left(\hat{y}_i-y_i\right)^2}{\sum_{i=1}^{N}\left(\hat{y}_i-\overline{y}\right)^2} \tag{12}$$

where $\hat{y}_i$ is the prediction result of the machine learning model, y_i is the value of the rolling experiment, and $\overline{y}$ is the average value of the rolling experiment. All the above evaluation metrics are dimensionless. A higher R^2 value closer to 1, along with smaller values of MAE, MRE, and MSE, indicates the improved accuracy and stability of the model.

3 Results and discussion

3.1 Prediction of UTS

The comparison of four machine learning models for predicting the UTS output results is shown in Fig. 5. Figure 5(a) displays the experimental and predicted values, and Fig. 5(b) shows the MRE comparison chart. From Fig. 5(a), the predicted values of the BPNN and RF models significantly differ from the experimental values, and only fewer data fall within the error band of ±5 in contrast to the experimental values. In contrast, the predicted values of the SVR and KNN models show smaller differences from the experimental values, and most of the predicted values fall within the error band of

±5 compared to the experimental values. Moreover, it can be found in Fig. 5(b) that the MRE lines of the BPNN and RF models exhibit greater fluctuations and are far away from the zero relative error dashed line, while the relative error lines of the SVR and KNN models show smaller fluctuations and are close to the zero relative error dashed line.

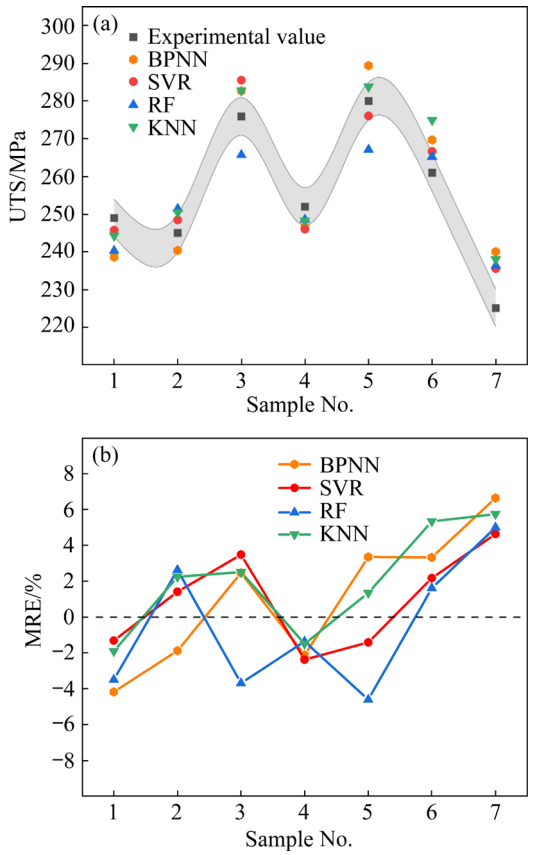

Fig. 5 Comparison of UTS prediction of four machine learning models: (a) Distribution of experimental and predicted values; (b) MRE

The bar chart of evaluation metrics for the four machine learning models predicting the UTS is shown in Fig. 6. The SVR model can well predict the UTS, with the smallest MAE of 6.05, the smallest MRE of 2.40%, and the smallest MSE of 43.93. The KNN model has a performance close to SVR, with an MAE of 7.36, an MRE of 2.94%, and an MSE of 70.01. The evaluation metrics for the BPNN and RF models are relatively high, indicating larger errors between predicted and experimental values and poorer predictive performance. The ranking of predictive ability for the models is SVR > KNN > RF > BPNN.

The comparison of the determination coefficients of the four machine learning models for predicting UTS is depicted in Fig. 7. From Fig. 7, the training determination coefficient (Train_R^2) ranking for each model from high to low is SVR > KNN > BPNN > RF. A Train_R^2 closer to 1 indicates a better fit of the model to the training data. The testing determination coefficient (Test_R^2) ranking for each model from high to low is SVR > KNN > BPNN > RF. A Test_R^2 closer to 1 signifies a better fit of the model to the prediction data and indicates better generalization performance. The overall determination coefficient (Total_R^2) ranking for each model from high to low is SVR > KNN > BPNN > RF. A Total_R^2 closer to 1 indicates a better fit of the model to the overall data and better generalization performance. However, the Train_R^2 close to 1 does not necessarily mean that the model is the best, and it could indicate overfitting, which may result in poor predictive performance on new data. Therefore, when the model is evaluated, it is essential to consider both Train_R^2 and Test_R^2, that is, Total_R^2, to ensure that the model has good overall performance. In conclusion, when the UTS of AZ31 magnesium alloy rolled sheets is predicted using the four machine learning models, the performance of the SVR and KNN models is better than that of the BPNN and RF models. The ranking of model performance from high to low is SVR > KNN > BPNN > RF, with the Total_R^2 values of 0.9296, 0.8785, 0.8509, and 0.8372, respectively.

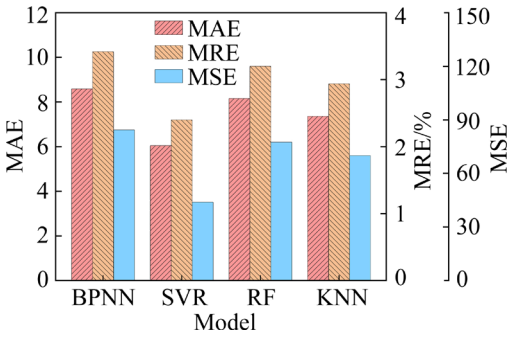

Fig. 6 Histogram of evaluation metrics of four machine learning models for predicting UTS

3.2 Prediction of EL

The comparison chart of the EL prediction by four machine learning models is shown in Fig. 8. The experimental and predicted values are displayed in Fig. 8(a), while the MRE comparison chart is illustrated in Fig. 8(b). It can be observed in Fig. 8(a) that the prediction values from the BPNN and RF models significantly differ from the experimental values. While the prediction values from the SVR

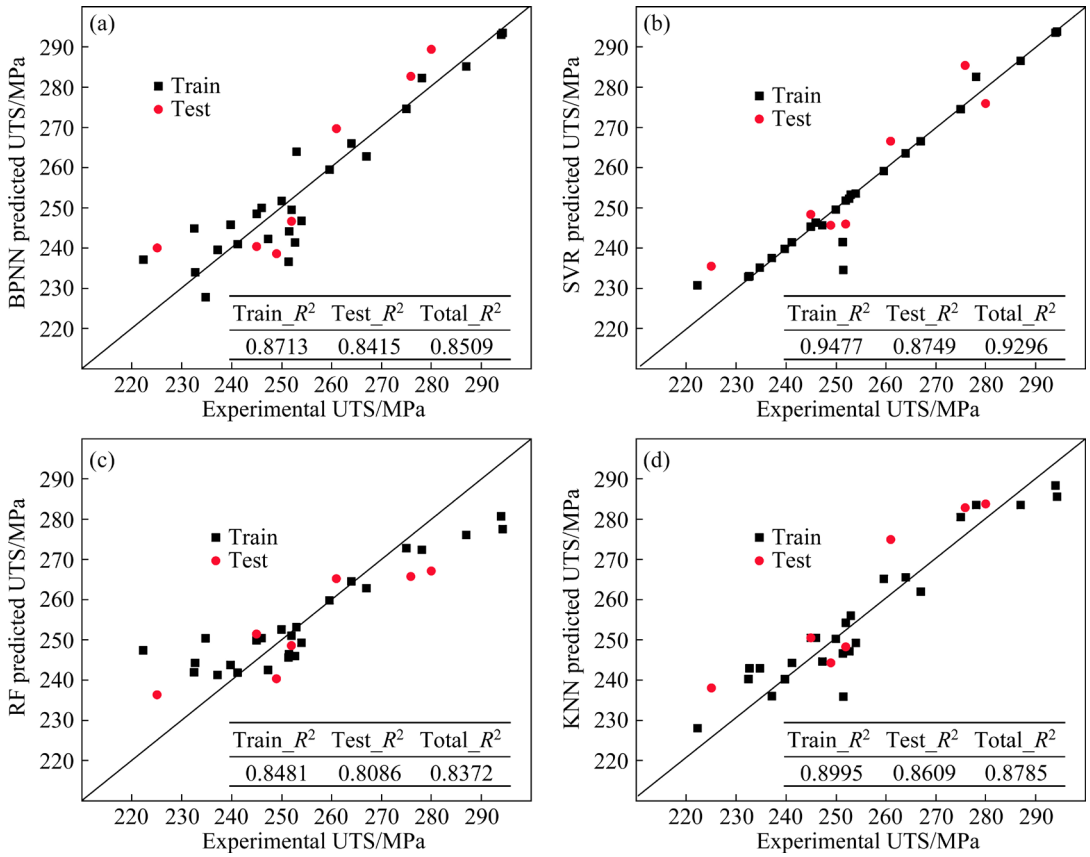

Fig. 7 Comparison of determination coefficients of four machine learning models for predicting UTS: (a) BPNN; (b) SVR; (c) RF; (d) KNN

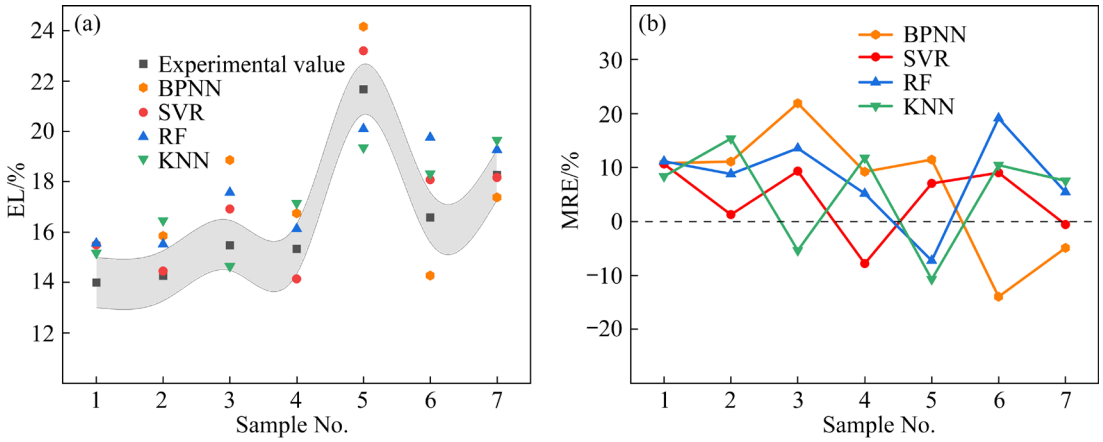

Fig. 8 Comparison of EL prediction of four machine learning models: (a) Distribution of experimental and predicted values; (b) Relative error comparison chart

model show smaller deviations from the experimental values. As shown in Fig. 8(b), the MRE lines of the KNN, BPNN, and RF models exhibit larger fluctuations and are far from the zero relative error dashed line. Conversely, the relative error line of the SVR model shows smaller fluctuations and is close to the zero relative error dashed line.

The bar chart of evaluation metrics of the four machine learning models for predicting the EL is shown in Fig. 9. The SVR model can well predict the EL, with the smallest MAE of 1.06, the smallest MRE of 6.53%, and the smallest MSE of 1.48. The KNN model shows a performance close to SVR, with an MAE of 1.63, an MRE of 9.95%, and an

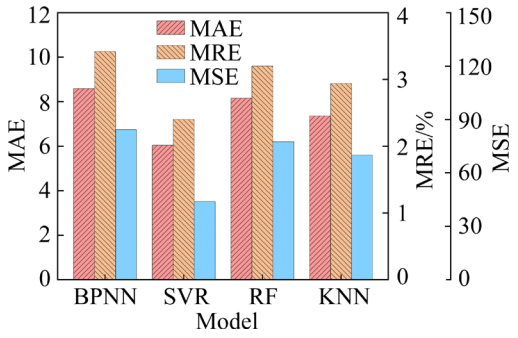

Fig. 9 Histogram of evaluation metrics of four machine learning models for predicting EL

MSE of 2.92. Furthermore, the evaluation metrics for the BPNN and RF models are relatively high, indicating poorer predictive performance. Therefore, the ranking of predictive ability for the models from high to low is SVR > KNN > RF > BPNN.

The comparison of the determination coefficients of the four machine learning models for predicting EL is depicted in Fig. 10. The ranking of the Train_R^2 for each model from high to low is SVR > RF > KNN > BPNN; the Test_R^2 from high to low is SVR > RF > BP > KNN, and the Total_R^2 from high to low is SVR > RF > BPNN > KNN. Overall, when the EL of AZ31 magnesium alloy rolled sheets is predicted by applying the four machine learning models, the SVR and RF models exhibit excellent performance, while the BPNN and RF models show poorer performance. The ranking of model performance from high to low is SVR > RF > BPNN > KNN, with the Total_R^2 values of 0.9136, 0.7208, 0.6834, and 0.6794, respectively.

3.3 PCC analysis results

PCC is a statistical measure used to assess the degree of linear correlation between two variables. It ranges from −1 to 1, where 0 indicates no linear correlation, 1 indicates a perfect positive correlation, and −1 indicates a perfect negative correlation. The formula is given in the following equation [53]:

$$r=\frac{\sum_{i=1}^{N}(x_i-\bar{X})(y_i-\bar{Y})}{\sqrt{\sum_{i=1}^{N}(x_i-\bar{X})^2}\sqrt{\sum_{i=1}^{N}(x_i-\bar{Y})^2}} \tag{13}$$

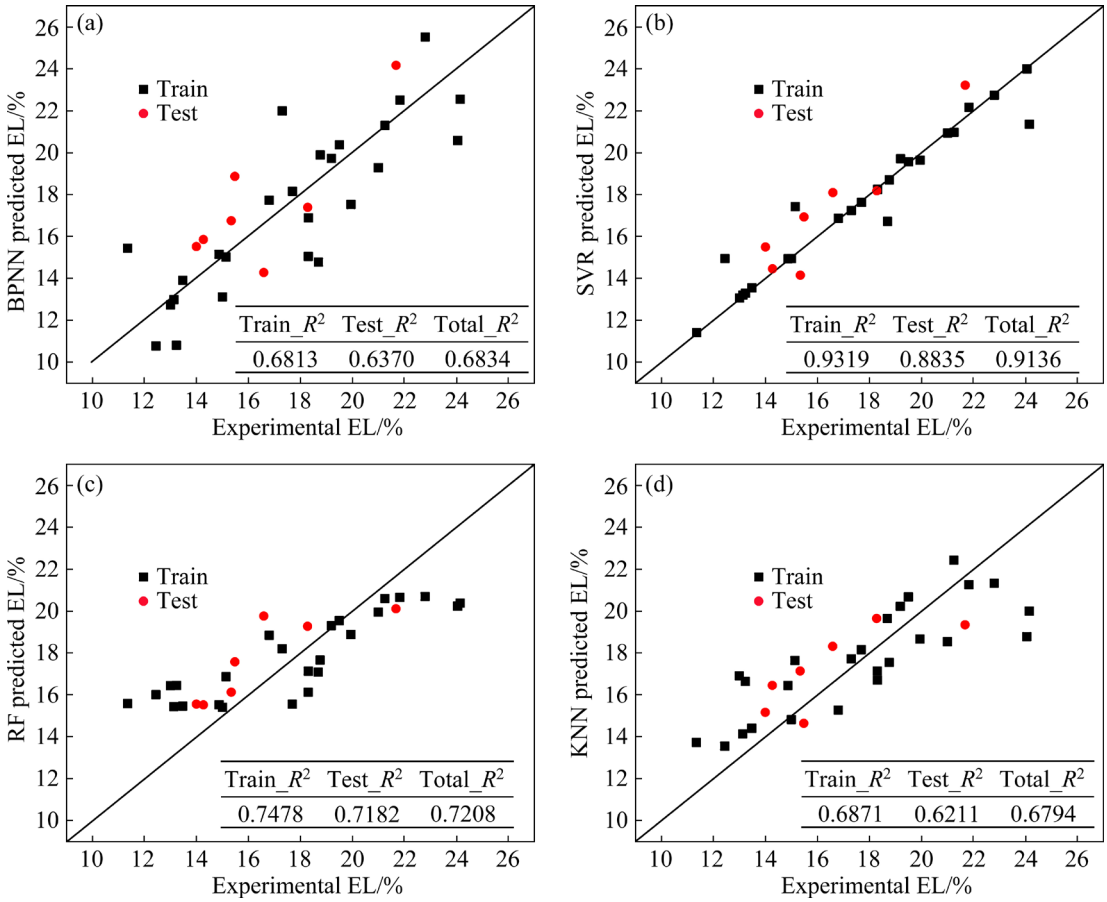

Fig. 10 Comparison of determination coefficient of four machine learning models for predicting EL: (a) BPNN; (b) SVR; (c) RF; (d) KNN

where r is the Pearson correlation coefficient, $\overline{X}$ is the sample mean of the sample set x, and $\overline{Y}$ is the sample mean of the sample set y. Figure 11 displays a heat map of the PCC between the rolling process parameters and the mechanical properties of AZ31 magnesium alloy rolled sheets, with the highlighted green boxes indicating the correlation coefficient results.

As shown in Fig. 11, strain rate and reduction show a moderate correlation with the UTS, while rolling temperature presents a non-linear correlation. Specifically, there is a negative correlation between strain rate and UTS, as well as a positive correlation between reduction and UTS. The correlations can be demonstrated in the following aspects. The UTS is influenced by the grain size, and when the reduction is constant, the grain size is affected by the combined effects of rolling temperature and strain rate. At medium-to-high-strain-rate, the significant plastic deformation occurs, and the conversion of plastic deformation work into heat energy leads to an increase in plastic deformation temperature. Temperature rise caused by plastic deformation work increases with the increase in strain rate, and the increase in temperature causes an increase in recrystallized grain size, which exceeds the decrease in recrystallized grain size caused by the strain rate. In general, the grain size increases with the increase in strain rate. According to the Hall−Petch formula [54], the UTS of the material shows a decreasing trend with the increase of strain rate, so there is a negative correlation between strain rate and UTS. Furthermore, as the reduction increases, the material undergoes more plastic deformation, leading to an increase in the degree of recrystallization and grain refinement. According to the Hall−Petch formula, the UTS of the material increases, so there is a positive correlation between reduction and UTS.

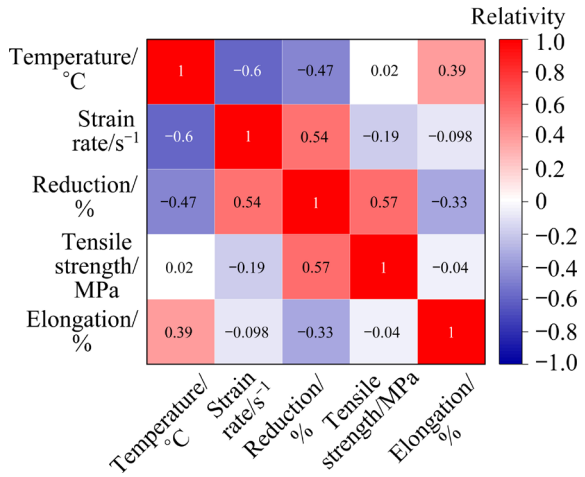

Fig. 11 Heat map of PCC

Rolling temperature is moderately correlated with EL, reduction is weakly correlated with EL, and strain rate is non-linearly correlated with EL. Herein, rolling temperature is positively correlated with EL, while reduction is negatively correlated with UTS. The correlations can be analyzed in the following ways: As rolling temperature increases, the internal thermal activation energy of the material increases, leading to larger atomic vibrational amplitudes and lower interatomic bonding forces. This reduces the hindrance of dislocations within the grains, as well as enhances the plastic deformation capability of the material. This results in a larger EL, indicating a positive correlation between rolling temperature and EL. Furthermore, as reduction increases, the material experiences greater pressure, causing distortion in the internal lattice structure and shortening the average distance between atoms. This increases the interatomic interaction forces, making the material harder and more brittle, thereby decreasing EL. On the other hand, with the increase of reduction, the dislocation density within the material increases. These dislocations act as obstacles, hindering the slip movement of atoms when subjected to external forces, making it difficult for the material to deform under stress, and resulting in a decrease in plastic deformation capability, namely a decrease in the EL. Therefore, there is a negative correlation between reduction and EL.

3.4 SHAP method analysis results

The SHAP is based on the Shapley value concept from game theory. It predicts different feature values and calculates contributions to determine each impact of features on the prediction. This method can provide visual explanations for machine learning models, aiding in understanding and interpreting model predictions. It instantiates an explainer by parsing the original model and then calculates the SHAP value corresponding to each feature for each sample through the explainer. Additionally, the method can capture nonlinear relationships, addressing the limitation of PCC in conducting nonlinear correlation analysis. Therefore, it can be used to validate the linear results obtained from PCC and reveal the correlation between temperature and UTS as well as strain rate and EL in

Section 3.3. In this study, the SHAP was established by invoking a Python toolkit based on the SVR model that performed well in overall prediction. Herein, the SHAP method was used to analyze the contribution of each feature to the SVR model output.

The |SHAP value| that represents the absolute value of the SHAP value corresponding to different features in the model concerning the UTS and EL outputs is displayed in Figs. 12(a) and 13(a), respectively. The impact of each feature on the machine learning model can be assessed by comparing the |SHAP value| of each feature. A higher SHAP value indicates a higher impact of this feature on the machine learning model. The distribution of SHAP values for different input features in the model concerning the UTS and EL outputs is shown in Figs. 12(b) and 13(b), respectively. In Figs. 12(b) and 13(b), each row represents a feature, and each point represents a sample point in the training process of the model. The horizontal axis indicates the size of the SHAP value, increasing from left to right, and this indicates the correlation of the feature with the output changing from negative to positive. The vertical axis represents the size of the feature value assigned to the feature during the training process of the model, with darker red indicating higher feature values and darker blue indicating lower feature values. Moreover, the correlation of each feature with the mechanical properties of AZ31 magnesium rolled sheet can also be derived, with the correlation decreasing from top to bottom. If the majority of red sample points are located on the right side, it indicates a positive correlation between this feature and the target attribute; otherwise, it is a negative correlation.

As shown in Fig. 12(a), it can be observed that the feature of reduction plays an important role in the SVR model output of the UTS, followed by the features of strain rate and rolling temperature. In Fig. 12(b), it can be seen that there is a strong positive correlation between reduction and UTS (plenty of red points are on the right side of SHAP=0) and a weak negative correlation between strain rate and UTS (few red points are on the left side of SHAP=0), while the correlation between rolling temperature and UTS is not significant (red points are evenly distributed on both sides of SHAP=0). In conclusion, there is a positive correlation between reduction and UTS, a negative correlation between strain rate and UTS, and an insignificant correlation between rolling temperature and UTS, while strain rate and reduction have a greater impact on the UTS compared to rolling temperature. These conclusions complement and substantiate the results of the PCC analysis.

It can be seen from Fig. 13(a) that the feature of strain rate plays an important role in the SVR model output of the EL, followed by the features of rolling temperature and reduction. In Fig. 13(b), it can be observed that there is a weak negative correlation between reduction and EL (few red points are on the left side of SHAP=0), and the correlation between strain rate and EL, as well as rolling temperature and EL, is not significant (red points are evenly distributed on both sides of SHAP=0). In conclusion, there is a negative correlation between reduction and EL, and strain rate and rolling temperature have a greater impact on the EL compared to the reduction, supplementing and validating the results of the PCC analysis.

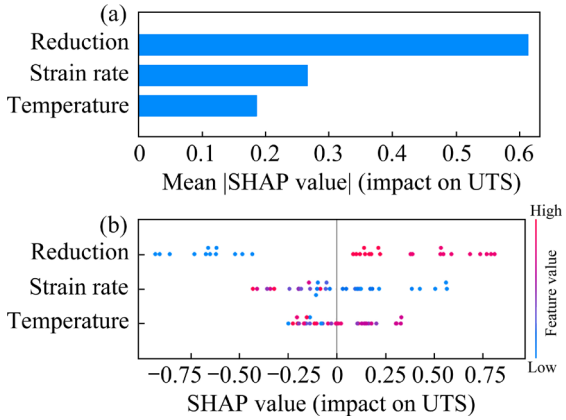

Fig. 12 Analysis results of SHAP value of UTS output: (a) Mean |SHAP value| for each input parameter; (b) Distribution of SHAP values for each input parameter

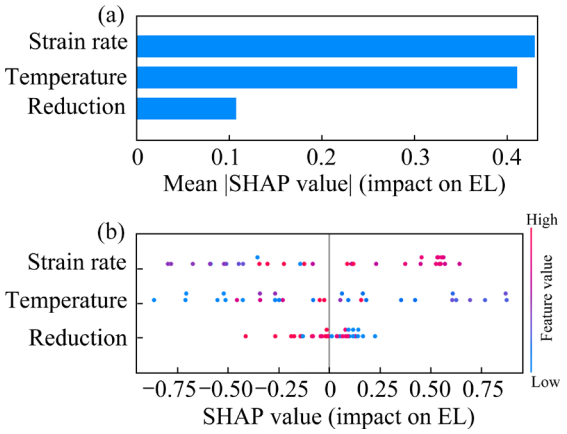

Fig. 13 Analysis results of SHAP value of EL output: (a) Mean |SHAP value| for each input parameter; (b) Distribution of SHAP values for each input parameter

4 Conclusions

(1) The optimal parameters for the BP, SVR, RF, and KNN machine learning models were determined by the LOOCV and parameter tuning. The KNN model performed well in predicting the UTS of AZ31 magnesium alloy rolled sheets, but Total_R^2 was low when predicting EL. The SVR model performed well in predicting both the UTS and EL in AZ31 magnesium alloy rolled sheets and better in contrast to other models. The MAE, MRE, MSE, and Total R^2 for UTS were 6.05, 2.40%, 43.93, and 0.9296, respectively, and the MAE, MRE, MSE, and Total R^2 for EL were 1.06, 6.53%, 1.48, and 0.9136, respectively.

(2) According to the PCC results, strain rate and reduction were negatively and positively correlated with UTS, respectively. Rolling temperature and reduction were positively and negatively correlated with EL, respectively. By PCC combined with the theory of magnesium alloy rolling forming, the relationship between the rolling process and the mechanical properties of AZ31 magnesium alloy rolled sheets was demonstrated.

(3) The SHAP, which could explain the output of the machine learning model, was established based on the SVR model. Through the SHAP method, it was inferred that the features of reduction and strain rate played an important role in the SVR model output for UTS and EL, respectively. Combining this with the PCC analysis, it was determined that strain rate and reduction on UTS had greater impact compared to rolling temperature, and strain rate and rolling temperature had a greater impact on EL compared to reduction.

CRediT authorship contribution statement

Bi-wu ZHU: Methodology, Investigation; **Hao JIANG:** Methodology, Investigation, Writing − Original draft; **Qiu-ping YI:** Methodology, Investigation; **Xiao LIU:** Supervision, Writing − Review & editing; **Jian-zhao WU:** Investigation; **Wen-hui LIU:** Investigation; **Cong-chang XU:** Investigation; **Luo-xing LI:** Investigation; **Ke HU:** Investigation.

Declaration of competing interest

The authors declare that they have no known competing financial interests or personal relationships that could have appeared to influence the work reported in this paper.

Acknowledgments

This study was supported by the National Natural Science Foundation of China (Nos. 52471132, 52475356, 52071139, U21A20130), the National Social Science Fund of China (No. 21BJL075), the Natural Science Foundation of Fujian Province for Distinguished Young Scholars, China (No. 2024J010031), and the Natural Science Foundation of Chongqing, China (No. CSTB2023NSCQ-MSX0886).

References

[1] WANG Jian, WANG Chen, RAO Wei-feng, JUNG In-ho. Design and characterization of biodegradable Mg−Zn−Ag metallic glasses [J]. Transactions of Nonferrous Metals Society of China, 2024, 34(9): 2814−2827.

[2] TAM K J, VAUGHAN M W, SHEN L M, KNEZEVIC M, KARAMAN I, PROUST G. Modelling dynamic recrystallisation in magnesium alloy AZ31 [J]. International Journal of Plasticity, 2021, 142: 102995.

[3] PRASAD S V S, PRASAD S B, VERMA K, MISHRA R K, KUMAR V, SINGH S. The role and significance of magnesium in modern day research—A review [J]. Journal of Magnesium and Alloys, 2022, 10(1): 1−61.

[4] REN Xian-wei, HUANG Yuan-chun, ZHANG Xie-yi, LI Hao, ZHAO Yong-xing. Influence of shear deformation during asymmetric rolling on the microstructure, texture, and mechanical properties of the AZ31B magnesium alloy sheet [J]. Materials Science and Engineering: A, 2021, 800: 140306.

[5] XU Jian, ZHENG Jie, LIU Wan-er, HUANG You-wang, YAN Zhao-ming, ZHANG Zhi-min, WANG Qiang, XUE Yong. Recrystallization behavior and strengthening mechanism of extruded Mg−Gd−Y−Zn−Zr alloy with different pre-aged states [J]. Transactions of Nonferrous Metals Society of China, 2024, 34(2): 480−503.

[6] RAKSHITH M, SEENUVASAPERUMAL P. Review on the effect of different processing techniques on the microstructure and mechanical behaviour of AZ31 Magnesium alloy [J]. Journal of Magnesium and Alloys, 2021, 9(5): 1692−1714.

[7] LIU Xiao, WAN Quan-hui, ZHU Bi-wu, LIU Wen-hui, LI Luo-xing, XU Cong-chang, GUO Peng-cheng. Effect of low-angle grain boundary and twin on precipitation mechanism in pre-rolled AZ91 magnesium alloy [J]. Journal of Materials Science, 2024, 59(8): 3662−3675.

[8] ZHANG Zhi, ZHANG Jing-huai, WANG Wen-ke, LIU Shu-juan, SUN Bin, XIE Jin-su, XIAO Ting-xu. Unveiling the deformation mechanism of highly deformable magnesium alloy with heterogeneous grains [J]. Scripta Materialia, 2022, 221: 114963.

[9] XU Yan, ZHANG Xu-xing, LI Wei, HU Peng-hong, JIA Jian-bo, LUO Jun-ting. Ultrafine lamellar structure AM60B magnesium alloy sheet prepared by high strain rate rolling [J]. Materials Science and Engineering: A, 2020, 781: 139221.

[10] LIU Xiao, HE Dan-dan, ZHU Bi-wu, LIU Wen-hui, YE Fan, WEI Fuan, XU Cong-chang, LI Luo-xing. The ordered orientation gradient “sandwich” texture induced high strength−ductility in AZ31 magnesium alloy [J]. Scripta Materialia, 2024, 253: 116296.

[11] NAZEER F, LONG Jian-yu, YANG Zhe, LI Chuan.

Superplastic deformation behavior of Mg alloys: A review [J]. Journal of Magnesium and Alloys, 2022, 10(1): 97−109.

[12] LIU Xiao, LI Heng, HU Min-yue, ZHU Bi-wu, XIE Chao, ZHANG Xiao-feng, LIU Wen-hui. Effect of deformation mode on double-peak texture evolution in pre-twinning Mg−3Al−1Zn alloy during high-speed impacting loading [J]. Journal of Alloys and Compounds, 2023, 968: 172122.

[13] MAHESH B. Machine learning algorithms—A review [J]. International Journal of Science and Research, 2020, 9(1): 381−386.

[14] JORDAN M I, MITCHELL T M. Machine learning: Trends, perspectives, and prospects [J]. Science, 2015, 349(6245): 255−260.

[15] RUDIN C. Stop explaining black box machine learning models for high stakes decisions and use interpretable models instead [J]. Nature Machine Intelligence, 2019, 1(5): 206−215.

[16] HART G L W, MUELLER T, TOHER C, CURTAROLO S. Machine learning for alloys [J]. Nature Reviews Materials, 2021, 6(8): 730−755.

[17] FAN Jiang-bo, WANG Zhang-wei, LIU Chang-qi, SHI Duo-qi, YANG Xiao-guang. A tensile properties-related fatigue strength predicted machine learning framework for alloys used in aerospace [J]. Engineering Fracture Mechanics, 2024, 301: 110057.

[18] LI Z, LI S, BIRBILIS N. A machine learning-driven framework for the property prediction and generative design of multiple principal element alloys [J]. Materials Today Communications, 2024, 38: 107940.

[19] SUH J S, KIM Y M, YIM C D, SUH B C, BAE J H, LEE H W. Interpretable machine learning-based analysis of mechanical properties of extruded Mg−Al−Zn−Mn−Ca−Y alloys [J]. Journal of Alloys and Compounds, 2023, 968: 172007.

[20] XU Xue-nan, WANG Le-yun, ZHU Gao-ming, ZENG Xiao-qin. Predicting tensile properties of AZ31 magnesium alloys by machine learning [J]. JOM, 2020, 72(11): 3935−3942.

[21] DONG Shu-ya, WANG Ying-ying, LI Jin-ya, LI Yuan-yuan, WANG Li, ZHANG Jing-lai. Machine learning aided prediction and design for the mechanical properties of magnesium alloys [J]. Metals and Materials International, 2024, 30(3): 593−606.

[22] YANG Chen, REN Chang, JIA Yue-fei, WANG Gang, LI Min-jie, LU Wen-cong. A machine learning-based alloy design system to facilitate the rational design of high entropy alloys with enhanced hardness [J]. Acta Materialia, 2022, 222: 117431.

[23] ZHOU Xian, ZHENG Zhi-chun, LU Tian, XU Peng-cheng, CHANG Ting, LI Min-jie, LU Wen-cong. Interpretable machine learning assisted multi-objective optimization design for small molecule hole transport materials [J]. Journal of Alloys and Compounds, 2023, 966: 171440.

[24] WU Jian-zhao, LIAN Kun-lei, DENG Ye-lin, JIANG Ping, ZHANG Chao-yong. Multi-objective parameter optimization of fiber laser welding considering energy consumption and bead geometry [J]. IEEE Transactions on Automation Science and Engineering, 2022, 19(4): 3561−3574.

[25] KAMAL T, GOUTHAMA, UPADHYAYA A. Machine learning based sintered density prediction of bronze processed by powder metallurgy route [J]. Metals and Materials International, 2023, 29(6): 1761−1774.

[26] JI Shu-juan, WANG Xin, LYU T, LIU Xiao-jie, WANG Yuan-qing, HEINEN E, SUN Zhen-wei. Understanding cycling distance according to the prediction of the XGBoost and the interpretation of SHAP: A non-linear and interaction effect analysis [J]. Journal of Transport Geography, 2022, 103: 103414.

[27] HU Jing-xuan, FAN Tian-hui, TANG Xiao-lan, YANG Zhi-jie, REN Yu-jie. Nonlinear relations of urban morphology to thermal anomalies: A cross-time comparative study based on Grad-CAM and SHAP [J]. Ecological Indicators, 2024, 162: 112024.

[28] BALLESTER P L, CARDOSO T D A, MOREIRA F P, SILVA R A D, MONDIN T C, ARAUJO R M, KAPCZINSKI F, FREY B N, JANSEN K, SOUZA L D D M. 5-year incidence of suicide-risk in youth: A gradient tree boosting and SHAP study [J]. Journal of Affective Disorders, 2021, 295: 1049−1056.

[29] LIU Fu-bao, LIU Xiao, ZHU Bi-wu, YANG Hui, XIAO Gang, HU Ming-yue. Influence of microstructure and mechanical properties on formability in high strain rate rolled AZ31 magnesium alloy sheets [J]. Metals and Materials International, 2022, 28(6): 1361−1371.

[30] LIU Xiao, ZHU Bi-wu, WEI Fu-an, YANG Wei-cheng, LIU Wen-hui, LI Luo-xing, XU Cong-chang, GUO Peng-cheng. Heterogeneous lamella mixed grain structures of strength−ductility synergy in medium strain rate rolled AZ31 magnesium sheets [J]. Materials Science and Engineering: A, 2024, 916: 147387.

[31] LIU Xiao, YANG Wei-cheng, ZHU Bi-wu, WU Yuan-Zhi, TANG Chang-ping, LIU Wen-hui, SONG Yu-feng. Process and microstructure properties of multi-scale mixed crystal magnesium alloy prepared by medium strain rate rolling [J]. The Chinese Journal of Nonferrous Metals, 2023, 33(3): 678−688. (in Chinese)

[32] HUANG Jiang-lin, LI Yan-fu, XIE Min. An empirical analysis of data preprocessing for machine learning-based software cost estimation [J]. Information and Software Technology, 2015, 67: 108−127.

[33] RAHMAN A. Statistics-based data preprocessing methods and machine learning algorithms for big data analysis [J]. International Journal of Artificial Intelligence, 2019, 17(2): 44−65.

[34] SHEN Cheng, BAO Xue-jing, TAN Jiu-bin, LIU Shu-tian, LIU Zheng-jun. Two noise-robust axial scanning multi-image phase retrieval algorithms based on Pauta criterion and smoothness constraint [J]. Optics Express, 2017, 25(14): 16235−16249.

[35] ZHANG Shu-yuan, XU Jin-jun, LAI Tao, YU Yong, XIONG Wei-wei. Bond stress estimation of profiled steel-concrete in steel reinforced concrete composite structures using ensemble machine learning approaches [J]. Engineering Structures, 2023, 294: 116725.

[36] WANG Zhen, MU Lin, MIAO Hong-chao, SHANG Yan, YIN Hong-chao, DONG Ming. An innovative application of machine learning in prediction of the syngas properties of biomass chemical looping gasification based on extra trees regression algorithm [J]. Energy, 2023, 275: 127438.

[37] ZHANG Sha-sha, YUAN Yu-yu, YAO Zhong-hua, YANG Jin-cui, WANG Xin-yan, TIAN Jian-wei. Coronary artery disease detection model based on class balancing methods and LightGBM algorithm [J]. Electronics, 2022, 11(9): 1495.

[38] LIAO Heng-cheng, GAO Yuan, WANG Qi-gui, WILSON D. Development of viscosity model for aluminum alloys using

BP neural network [J]. Transactions of Nonferrous Metals Society of China, 2021, 31(10): 2978−2985.
[39] GOH A T C. Back-propagation neural networks for modeling complex systems [J]. Artificial Intelligence in Engineering, 1995, 9(3): 143−151.
[40] ZHU Cheng-peng, LI Chao, WU Di, YE Wan, SHI Shuang-xi, MING Hui, ZHANG Xiao-yong, ZHOU Ke-chao. A titanium alloys design method based on high-throughput experiments and machine learning [J]. Journal of Materials Research and Technology, 2021, 11: 2336−2353.
[41] LAABID Z, MOUMEN A, MANSOURI K, SIADAT A. Numerical study of the speed's response of the various intelligent models using the tansig, logsig and purelin activation functions in different layers of artificial neural network [J]. IAES International Journal of Artificial Intelligence, 2023, 12(1): 155.
[42] LI Xin, SHAN Guang-cun, ZHAO Hong-bin, SHEK C H. Domain knowledge aided machine learning method for properties prediction of soft magnetic metallic glasses [J]. Transactions of Nonferrous Metals Society of China, 2023, 33(1): 209−219.
[43] LIU Xiu-juan, XU Peng-cheng, ZHAO Juan-juan, LU Wen-cong, LI Min-jie, WANG Gang. Material machine learning for alloys: Applications, challenges and perspectives [J]. Journal of Alloys and Compounds, 2022, 921: 165984.
[44] MI Xiao-xi, DAI Li-li, JING Xue-rui, SHE Jia, HOLMEDAL B, TANG Ai-tao, PAN Fu-sheng. Accelerated design of high-performance Mg−Mn-based magnesium alloys based on novel Bayesian optimization [J]. Journal of Magnesium and Alloys, 2024, 12(2): 750−766.
[45] BREIMAN L. Random forests [J]. Machine Learning, 2001, 45(1): 5−32.
[46] DONG Long-jun, LI Xi-bing, PENG Kang. Prediction of rockburst classification using Random Forest [J]. Transactions of Nonferrous Metals Society of China, 2013, 23(2): 472−477.
[47] CHEN Tao, GAO Qian, YUAN Yuan, LI Ting-yu, XI Qian, LIU Ting-ting, TANG Ai-tao, WATSON A, PAN Fu-sheng. Coupling physics in machine learning to investigate the solution behavior of binary Mg alloys [J]. Journal of Magnesium and Alloys, 2022, 10(10): 2817−2832.
[48] ZHANG Shi-chao, LI Xue-long, ZONG Ming, ZHU Xiao-feng, WANG Rui-li. Efficient kNN classification with different numbers of nearest neighbors [J]. IEEE Transactions on Neural Networks and Learning Systems, 2018, 29(5): 1774−1785.
[49] ZHANG Shi-chao, LI Xue-long, ZONG Ming, ZHU Xiao-feng, CHENG De-bo. Learning *k* for KNN classification [J]. ACM Transactions on Intelligent Systems and Technology, 2017, 8(3): 43:1−43:19.
[50] UDDIN S, HAQUE I, LU H H, MONI M A, GIDE E. Comparative performance analysis of K-nearest neighbour (KNN) algorithm and its different variants for disease prediction [J]. Scientific Reports, 2022, 12(1): 6256.
[51] DANIELSSON P E. Euclidean distance mapping [J]. Computer Graphics and Image Processing, 1980, 14(3): 227−248.
[52] CHAI T, DRAXLER R R. Root mean square error (RMSE) or mean absolute error (MAE) [J]. Geoscientific Model Development Discussions, 2014, 7(1): 1525−1534.
[53] SALEHUDIN N B, KAHTAN H, ABDULLATEEF M A, AL-BASHIRI H. A proposed course recommender model based on collaborative filtering for course registration [J]. International Journal of Advanced Computer Science and Applications, 2019, 10(11): 162−168.
[54] ZHU S Q, YAN H G, CHEN J H, WU Y Z, SU B, DU Y G, LIAO X Z. Feasibility of high strain-rate rolling of a magnesium alloy across a wide temperature range [J]. Scripta Materialia, 2012, 67(4): 404−407.

AZ31 镁合金轧制板材力学性能的可解释机器学习预测模型

朱必武[1,2]，蒋 昊[2]，易秋平[3]，刘 筱[1,2,4]，吴剑钊[1]，刘文辉[1,2]，徐从昌[4]，李落星[4]，胡 克[5]

1. 集美大学 海洋装备与机械工程学院，厦门 361021；
2. 湖南科技大学 高功效轻合金构件成形技术及耐损伤性能评价湖南省工程研究中心，湘潭 411201；
3. 集美大学 财经学院，厦门 361021；
4. 湖南大学 重庆研究院，重庆 401135；
5. 广东海洋大学 材料科学与工程学院，阳江 529500

摘 要：为探究轧制工艺参数与 AZ31 镁合金轧制板材力学性能之间的复杂关系，采用留一法交叉验证(LOOCV)和参数循环优化了 4 个(BPNN、SVR、RF 和 KNN)机器学习模型的超参数，提出了一种基于机器学习和夏普利加法解释(SHAP)的可解释预测模型以及一种结合 SHAP 模型与皮尔逊相关系数(PCC)的分析方法。结果表明：在上述 4 种机器学习模型中，SVR 模型能够同时准确地预测极限抗拉强度(UTS)和伸长率(EL)；通过 PCC 结合镁合金轧制成形机理发现，应变速率和下压量分别与 UTS 呈负相关和正相关，轧制温度和下压量分别与 EL 呈正相关和负相关；通过可解释 SVR 机器学习模型输出结果的 SHAP 方法发现，下压量和应变速率分别在 UTS 和 EL 输出中发挥了重要作用；结合 SHAP 与 PCC 分析发现，应变速率和下压量比轧制温度对 UTS 的影响更大，而应变速率和轧制温度比下压量对 EL 的影响更大。

关键词：AZ31 镁合金；轧制工艺；力学性能；机器学习；夏普利加法解释

(Edited by Wei-ping CHEN)